



LAWRENCE
LIVERMORE
NATIONAL
LABORATORY

The LLNL/UCLA High Gradient Inverse Free Electron Laser Accelerator

J. T. Moody, P. Musumeci, G. Anderson, S. Anderson,
S. Betts, S. Fisher, D. Gibson, A. Tremaine, S. Wu

December 7, 2012

Advanced Accelerator Concepts Workshop
Austin, TX, United States
June 10, 2012 through June 15, 2012

Disclaimer

This document was prepared as an account of work sponsored by an agency of the United States government. Neither the United States government nor Lawrence Livermore National Security, LLC, nor any of their employees makes any warranty, expressed or implied, or assumes any legal liability or responsibility for the accuracy, completeness, or usefulness of any information, apparatus, product, or process disclosed, or represents that its use would not infringe privately owned rights. Reference herein to any specific commercial product, process, or service by trade name, trademark, manufacturer, or otherwise does not necessarily constitute or imply its endorsement, recommendation, or favoring by the United States government or Lawrence Livermore National Security, LLC. The views and opinions of authors expressed herein do not necessarily state or reflect those of the United States government or Lawrence Livermore National Security, LLC, and shall not be used for advertising or product endorsement purposes.

THE LLNL/UCLA HIGH GRADIENT INVERSE FREE ELECTRON LASER ACCELERATOR

J.T. Moody*, P. Musumeci*, G. Anderson†, S. Anderson†, S. Betts†, S. Fisher†, D. Gibson†, A. Tremaine† and S. Wu†

*Department of Physics and Astronomy, UCLA, Los Angeles California, 90095, USA

†Lawrence Livermore National Laboratory

Abstract. We describe the Inverse Free Electron Accelerator currently under construction at Lawrence Livermore National Lab. Upon completion of this accelerator, high brightness electrons generated in the photoinjector blowout regime and accelerated to 50 MeV by S-band accelerating sections will interact with > 4 TW peak power Ti:Sapphire laser in a highly tapered 50 cm undulator and experience an acceleration gradient of > 200 MeV/m. We present the final design of the accelerator as well as the results of start-to-end simulations investigating preservation of beam quality and tolerances involved with this accelerator.

Keywords: Laser based acceleration, Undulator

PACS: 29.20.Ej, 41.75.Fr, 41.75.Ht, 29.27.Ac

INTRODUCTION

Previous work has shown that acceleration of photoinjector electron beams via an inverse free electron laser interaction is viable both in maximum energy gain and in trapping [1], [2] up to GeV energy. Such a compact accelerator has applications ranging from x ray FEL to inverse Compton scattering. In this interaction a relativistic electron beam is co-propagated through a planar undulator with a high power laser. The interaction in 1-D can be described by the following equations of motion.

$$\frac{d\gamma}{dz} = \frac{1}{2\gamma} k K_L J J \sin \Psi \quad (1)$$

$$\frac{d\Psi}{dz} = k_w - \frac{k}{2\gamma^2} \left(1 + \frac{K^2}{2}\right) \quad (2)$$

Here k is $2\pi/\lambda$, K_L , also known as a_0 , is the radiation parameter equal to $eE_0\lambda/2\pi mc^2$ and E_0 is the peak radiation electric field, m is the electron mass, and c is the speed of light. K is the undulator strength parameter and is equal to $eB_w\lambda_w/2\pi mc^2$ and B_w is the peak undulator magnetic field. JJ is the coupling factor of the planar undulator, γ is electron beam energy scaled by its rest mass, and Ψ is the pondermotive phase, defined by $(k + k_w)z - \omega t$.

The undulation of the electron beam allows it to couple to the laser's electric field. The parameters of the undulator can be selected such that a maximum energy exchange between the electron beam and laser field occurs, which happens to be the point at which the pondermotive phase is stationary. This resonance condition is:

$$\lambda = \frac{\lambda_u \left(1 + \frac{K^2}{2}\right)}{2\gamma^2} \quad (3)$$

Because the energy of the electron beam is increasing during the acceleration process, the undulator is tapered both in field and period such that the trapped electron beam remains on an acceleration curve from an initial energy of 50 MeV to a final energy of 200 MeV. This experiment differs from previous experiments in that it uses a higher peak power and higher repetition rate laser to interact with the electron beam. Previous simulations [3] have shown that the power of the laser must be 4 TW, which is obtained using 500 mJ compressed to 120 fs. Using a short laser makes temporal overlap a significant factor in the experiment and thus a short electron beam must be used in order to get a reasonable amount of electrons trapped and accelerated to 200 MeV. In this paper we describe start-to-end simulations of the electron beam from the photocathode, through the initial traditional rf accelerating sections up to

50MeV, through compression to 100 fs bunch length, and finally the acceleration. Some accelerator parameters and tolerances are discussed as well as a timing diagnostic to characterize and separate the temporal overlap factor in this experiment.

EXPERIMENTAL LAYOUT

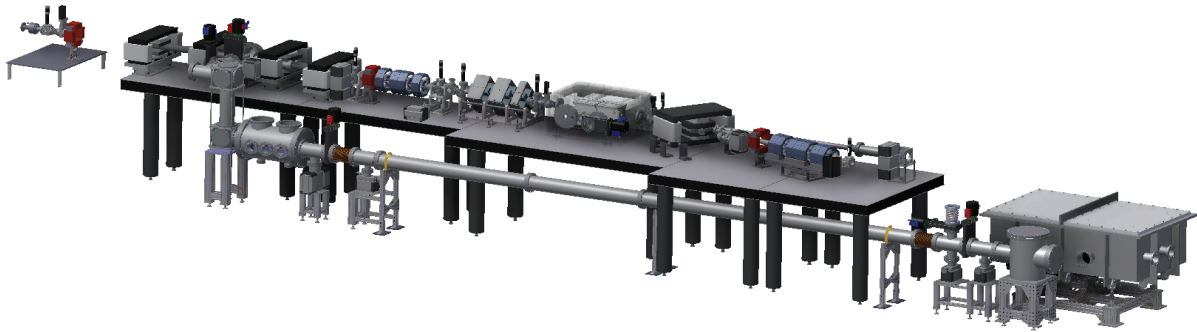


FIGURE 1. CAD model of the compressor and IFEL region of the LLNL IFEL experiment.

Laser Description

An 800 nm 30 mJ 200 ps laser pulse is split 90/10. Ten percent of the laser power is sent to a third harmonic generation (THG) section using nonlinear crystals and compressed to 100 fs to drive the photocathode and make the electron beam. The remaining 27 mJ is sent through a delay line to a main amplifier to be amplified to 700 mJ. This beam is then compressed to 500 mJ 120 fs in order to get sufficient field for trapping a reasonable 40% of the electron beam in the accelerating bucket. The laser is then sent through a transport in vacuum to a final focus off axis parabolic mirror selected such that the Rayleigh length is 3.5 cm with a spot size at the waist of 100 μm at the center of the undulator.

Electron Beam Description

The electron beam is emitted from a photocathode using the 266 nm generated by THG of the 800 nm. The electron beam is accelerated in a 1.6 Cell BNL/UCLA/SLAC style photogun to approximately 5 MeV. With a charge of 100 pC and initial radial spot size and bunch length of 1 mm and 120 fs, respectively, the electron beam is generated in the photoinjector "blowout" regime. In the blowout regime, a rapid space-charge dominated longitudinal expansion transforms the distribution of the beam to one that is approximately a uniformly filled ellipsoid. This reduces the space charge induced emittance growth both transversely and longitudinally at low energy before acceleration.

The beam is accelerated by two SLAC style accelerating sections to 50 MeV and a negative chirp is induced on the beam so that it can be compressed in a chicane. The beam is compressed to an rms time value of 60 fs and drifts to a final focus quadrupole triplet section to match into the undulator with a spot size of 25 μm with the waist at the center of the undulator.

After acceleration the beam is sent to a dipole spectrometer designed to measure entire energy range from 50 MeV to 200 MeV. The spectrometer's fluorescent screen can be extracted enough to allow the 200 MeV electrons to escape to a downstream quadrupole triplet and diagnostic screen where the emittance of the accelerated part of the beam can be measured via a quadrupole scan technique.

A computer assisted design (CAD) model drawing for the end of the LLNL/UCLA IFEL experiment is shown in Fig. 1. On the right the main laser compressor is seen as well as the transport to the left where the focusing OAP mirror and injection of the laser into the center of the chicane occurs. The electron beam approaches from the left

TABLE 1. Operating Point Parameters

Operating Point Parameters	
Initial Energy	50 MeV
Final Energy	200 MeV
Normalized Emittance	.6 mm-mrad
Charge	100 pC
Undulator Parameters	
λ_{u0}	1.5 cm
λ_{uf}	5.0 cm
$K_{initial}$	0.2
K_{final}	2.8
L_u	50 cm
K_L	.077

and is accelerated to 50 MeV as well as acquires a temporal energy chirp from SLAC style accelerating sections (not shown). The beam is then compressed in the chicane, runs through a timing diagnostic section, and finally is focused to be transversely matched into the undulator. Finally the spectrometer and quadrupole section can be seen on the right end of the optical table.

START TO END SIMULATION

To model the electron beam's interaction a cross platform simulation set was used. At low energy, where space charge is important, the beam is modeled using Parmela [4]. Parmela tracks the particles through the conventional rf acceleration to 50 MeV and the application of the chirp on the beam by the final rf accelerating section. During this section two quadrupole triplet sections keep the beam round and roughly collimated around a mm RMS. Elegant is then used to perform the simulations through the compression in the chicane. The embedded Saladin/Stupakov models for CSR are used to model the electron beam through the chicane and drift after, as well as the two final focus quadrupole triplets that match the beam into the undulator [5]. Finally the distribution is placed into cbeam [3], a particle tracking code developed by S. Anderson that tracks the particles through the undulator and IFEL interaction. Cbeam has an option for higher order Laguerre-Gaussian "supergaussian" modes, which are a more realistic representation of the applied laser as some saturation occurs during the amplification process transversely in the lasing medium.

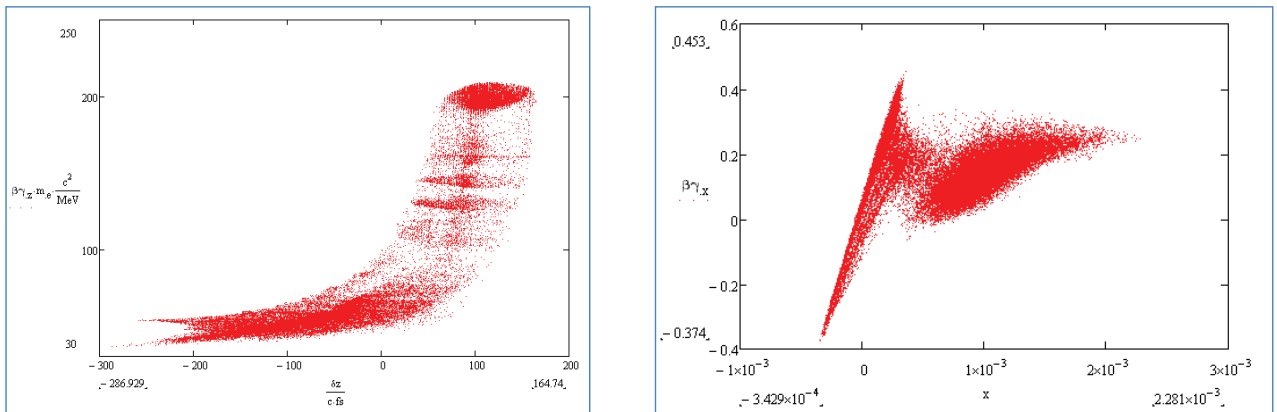


FIGURE 2. Longitudinal (left) and transverse (right) phase space plots of entire beam after acceleration

A sample longitudinal phase space plot resulting from the start to end simulation is shown in Fig. 2. Clearly acceleration of a part of the beam can be seen, as well as some structure due to particles slipping out of the accelerating bucket and falling into another. The captured part of the electron beam can be seen in the transverse phase space plot as the line on the left side of the plot. The rest of the beam is at different energies and thus has chromatic effects in

the undulator resulting in overall emittance growth of the beam. A histogram of the energy of the beam is shown in Fig. 3. This should closely match the image obtained on the spectrometer screen. This simulation is performed using the optimized parameters reported in Table 1.

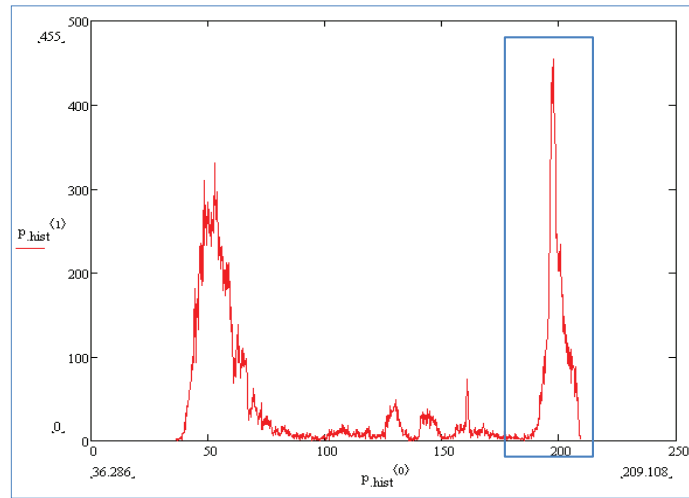


FIGURE 3. Histogram of Energy of beam at accelerator operating point. The accelerated beam is roughly 40% of the total beam can be seen as a spike at 200 MeV. The box is the distribution that was examined for the accelerated beam.

Characterization of the captured beam can be seen in Fig. 4. On the left side the transverse phase space can be seen. The transverse emittance in the horizontal plane is increased over that of the vertical transverse emittance (seen center) due to chromatic effects in the undulator and the energy spread of the captured beam. The longitudinal phase space can be seen at right, showing the energy spread and bunch length of the captured beam. The striated structure in the longitudinal phase space is due to the microbunching that occurs at 800nm.

The energy spread and emittance of the captured section can be better controlled by use of a prebunching section before the IFEL accelerating section. This will increase the amount of captured charge at a favorable accelerating phase that limits energy spread and emittance.

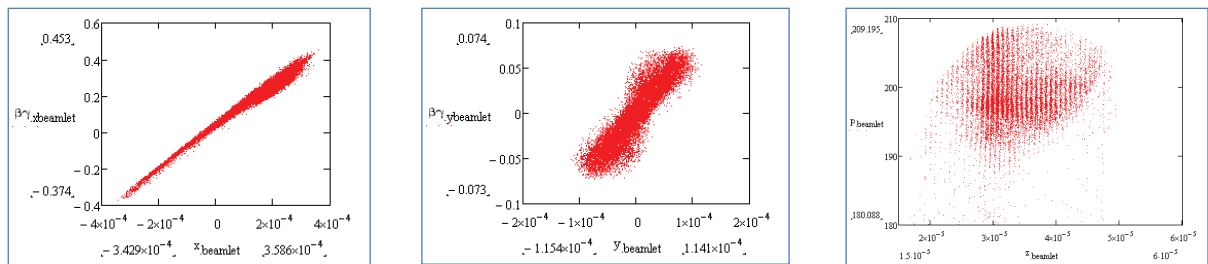


FIGURE 4. Captured Beam Phase Space: (Left) Transverse horizontal. (Center) Transverse vertical. (Right) Longitudinal Phase Space.

TOLERANCING AND TIMING DIAGNOSTIC

Tolerance Studies

To understand what we will likely observe during the experiment, parameters were varied around the operating point to determine tolerances for the accelerator. Tolerance studies were performed by varying parameters such as charge,

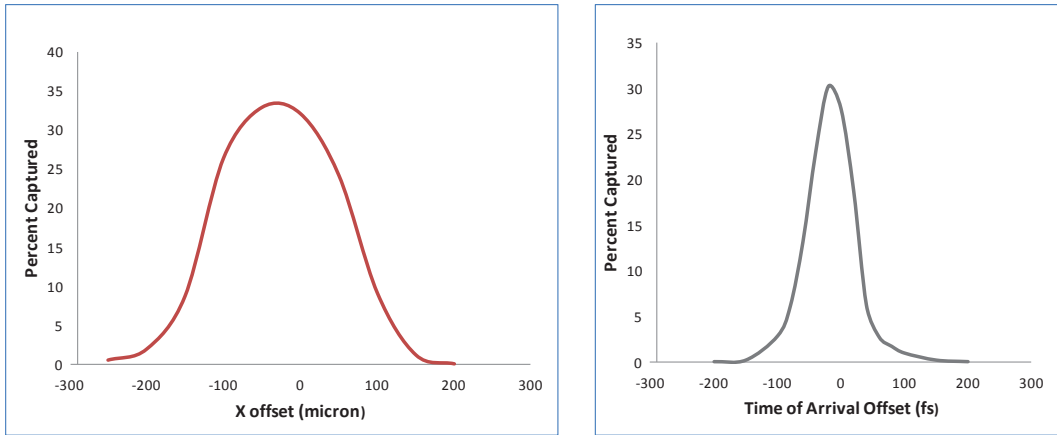


FIGURE 5. Spatial and TOA Tolerance Studies

initial transverse spatial offset into the beginning of the chicane, and time of arrival at the undulator. The figure of merit for these studies is the percentage of electrons captured and accelerated to energies above 180 MeV. The results of these studies can be seen in Fig. 5.

Timing Diagnostic

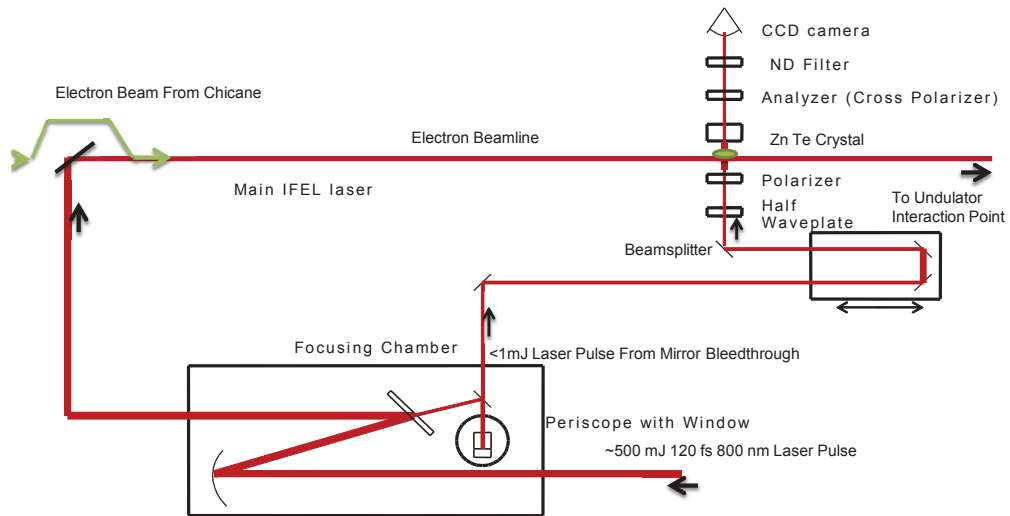


FIGURE 6. Timing Diagnostic Layout. Bleedthrough of one of the mirrors in the focusing chamber for 500 mJ laser yields a beam of roughly 1% of the power. This laser is transported through a delay stage to a cross polarizer setup where the field profile of the electron beam modulates its polarization. The transmission through the analyzer maps out the field of the electron beam. The centroid of the signal presents a relative time of arrival shot-to-shot.

As mentioned earlier, to keep the trapped electrons on the acceleration curve from 50 MeV to 200 MeV set by the undulator tapering profile, the electric field of the laser must be such that the laser's peak power is 4 TW, and the laser pulse length must be 120 fs. As can be seen from the tolerance studies the time of arrival (TOA) sensitivity is

on the order of 100 fs. With this level of sensitivity an online time of arrival diagnostic is useful in characterizing and understanding the accelerator's behavior.

Recent work done at UCLA has shown that spatially encoded electro-optic sampling (EOS) can act as a relative TOA diagnostic with a temporal resolution of 100 fs [6]. In that work a ZnTe crystal was placed 5 mm above the electron beam and the polarization of a laser traveling perpendicularly to the electron beam path is modulated by electron beam's field. By using crossed polarizers and a camera the spatial information of the electron beam's field is mapped in onto the transverse profile of the laser detected at the camera. This field map has the shape of a line set at the Cerenkov angle. If a lineout is taken longitudinally, the centroid can be measured. The change in the centroid of this lineout shot-to-shot gives information about the relative time of arrival of the electron beam. This measurement is non destructive and thus can be taken every shot at the standard repetition rate of the laser (10 Hz) while the accelerator is being operator. Thus the time of arrival can be directly correlated with the spectrometer measurements and accelerator can be characterized with respect to the time of arrival.

CONCLUSION AND OUTLOOK

The installation of the beamline and laser system for the experiment is now complete. First attempts at acceleration will occur during August 2012, characterization of the accelerator will extend through the end of FY 2012. Possibilities of inverse Compton scattering or x-ray FEL light source can happen as early as 2014.

REFERENCES

1. P. Musumeci et al., High Energy Gain of Trapped Electrons in a Tapered, Diffraction-Dominated Inverse-Free-Electron Laser, *Physical Review Letters*, 94:154801, (20 April 2005)
2. Kimura, W. D. et al. 2004b First demonstration of high-trapping efficiency and narrow energy spread in a laser-driven accelerator. *Phys. Rev. Lett.* 92, 054 801.
3. S. Anderson et al., Proc of PAC2011 (2011).
4. L.Young and J. Billen, The Particle Tracking Code PARMELA, PAC03 Proceedings, May 2003
5. M. Borland, Selegant: A Flexible SDDS-Compliant Code for Accelerator Simulation, Advanced Photon Source LS-287, September 2000.
6. C. M. Soby, et al, *Phys. Rev. ST Accel. Beams* 13, 022801 (2010).

Prepared by LLNL under Contract DE-AC52-07NA27344